International Journal of Plasticity 50 (2013) 94–108

Contents lists available at SciVerse ScienceDirect

International Journal of Plasticity

journal homepage: www.elsevier.com/locate/ijplas

# Dislocation density based model for plastic deformation and globularization of Ti-6Al-4V

Bijish Babu *, Lars-Erik Lindgren

*Mechanics of Solid Materials, Luleå University of Technology, SE-971 87 Luleå, Sweden*

ARTICLE INFO

*Article history:*
Received 10 July 2012
Received in final revised form 4 April 2013
Available online 25 April 2013

*Keywords:*
Dislocations
Vacancies
Diffusion
Dislocation glide
Climb

ABSTRACT

Although Ti-6Al-4V has numerous salient properties, its usage for certain applications is limited due to the challenges faced during manufacturing. Understanding the dominant deformation mechanisms and numerically modeling the process is the key to overcoming this hurdle. This paper investigates plastic deformation of the alloy at strain rates from 0.001 $s^{-1}$ to 1 $s^{-1}$ and temperatures between 20 °C and 1100 °C. Pertinent deformation mechanisms of the material when subjected to thermo-mechanical processing are discussed. A physically founded constitutive model based on the evolution of immobile dislocation density and excess vacancy concentration is developed. Parameters of the model are obtained by calibration using isothermal compression tests. This model is capable of describing plastic flow of the alloy in a wide range of temperature and strain rates by including the dominant deformation mechanisms like dislocation pile-up, dislocation glide, thermally activated dislocation climb, globularization, etc. The phenomena of flow softening and stress relaxation, crucial for the simulation of hot forming and heat treatment of Ti-6Al-4V, can also be accurately reproduced using this model.



## 1. Introduction

Ti-6Al-4V has good specific strength, toughness and corrosion resistance, which makes it attractive for applications in aerospace, pressure vessels, surgical implants, etc. Components for these applications have precise requirements on mechanical and physical properties (James and Lutjering, 2003). Furthermore, this alloy has a narrow temperature and strain rate window of workability (Kailas et al., 1994; Seshacharyulu et al., 2002). Optimization of the process parameters to satisfy the requirements on the component can be enabled by simulation. This work is part of a project aimed at performing finite element simulations of a manufacturing process chain involving hot-forming, welding, machining, metal deposition and heat treatment of Ti-6Al-4V components (Babu and Lundbäck, 2009; Tersing et al., 2012).

Manufacturing process chain simulations can compute the cumulative effect of the various processes by following the material state through the whole chain and give a realistic prediction of the final component. Capacity to describe material behavior in a wide range of temperatures and strain rates is crucial for this task. Such a model should be based on the dominant deformation mechanisms of the material.

Many different approaches were followed by researchers in formulating a physically based model for metal plasticity. Since the discrete dislocation modeling approach is computationally too expensive for the manufacturing process simulation, averaged dislocation density models are only discussed here. Initial attempts to develop dislocation density based models for metal plasticity were made by Kocks (1966), Bergström (1970), Bergström and Roberts (1973), Roberts and Bergström

* Corresponding author. Tel.: +46 (0) 70 419 78 17; fax: +46 920 492228.
*E-mail addresses:* bijish.babu@ltu.se (B. Babu), lars-erik.lindgren@ltu.se (L.-E. Lindgren).
*URL:* http://www.ltu.se/research/subjects/Materialmekanik (B. Babu).

0749-6419/$ - see front matter © 2013 Elsevier Ltd. All rights reserved.
http://dx.doi.org/10.1016/j.ijplas.2013.04.003

(1973), Kocks et al. (1975), Mecking and Estrin (1980), etc. These initial attempts to model basic material physics were later developed to include more detailed and complex mechanisms. Bergström (1983) partitioned dislocation density into mobile and immobile. Another approach followed by Estrin et al. (1998) is to split dislocations into low dislocation density channels and high dislocation density walls with separate evolution equations. Feaugas (1999), Feaugas and Gaudin (2001) extended this to account for kinematic hardening by separating the immobile dislocation density to walls and channels. Barlat et al. (2011) used a similar framework with forest and reverse dislocation densities to describe the Bauschinger effect. Statistically Stored Dislocations (SSD) and Geometrically Necessary Dislocations (GND) used by Arsenlis et al. (2004) and Cheong et al. (2005) are fundamentally similar to Estrin's model (Estrin et al., 1998).

Another approach is to partition dislocation densities into separate quantities for each active slip system useful for crystal plasticity models. For NiAl crystals, Busso and McClintock (1996) described the microstructure and flow characteristics during deformation based on the density and polarity of the dislocation structure. Peeters et al. (2001) proposed a model for bcc crystals which accounts for dislocation ensembles represented by three directionally sensitive dislocation densities generated during changing strain paths. For HCP crystals, Beyerlein and Tomé (2008) introduced separate hardening laws for each slip and twinning mode which are sensitive to temperature and rate.

Various approaches were employed by researchers to model the constitutive behavior of Ti-6Al-4V. Combining the Cingara model during hardening and JMAK model during softening, Shafaat et al. (2011) proposed an empirical flow stress model for Ti-6Al-4V. A similar approach was followed by Karpat (2011) by mixing a modified Johnson–Cook model for hardening and a hyperbolic model for softening which is used during machining simulation of Ti-6Al-4V. A simulated microstructure-based probabilistic framework has been used by Przybyla and McDowell (2011) for Ti-6Al-4V to model fatigue crack formation. Khan and Yu (2012), Khan et al. (2012) developed an anisotropic yield criterion for Ti-6Al-4V based on the KHL model. Dislocation density based models have been used by Nemat-Nasser et al. (1999) for commercially pure Titanium and Picu and Majorell (2002) and Gao et al. (2011) for Ti-6Al-4V. None of them has included the effects of vacancy evolution and globularization (grain coarsening).

This paper extends the model used by Lindgren et al. (2008) by including the effects of enhanced diffusivity. Further, a model for globularization that is responsible for flow-softening and stress relaxation is added. Isothermal test data is used in this paper to calibrate the model and therefore, the phase changes of the alloy are ignored.

Chaboche (2008) presented a review of the plastic and viscoplastic models, and Horstemeyer and Bammann (2010) showed the evolution and history of the internal state variable theory in plasticity. These two references show categorically where the current model stands in the family of the established constitutive theories. The constitutive model developed here for computing the yield strength can be used along with the Finite Element Method to solve thermo-mechanical problems of any dimension. The model is calibrated using compression tests and it is assumed that the material behavior is isotropic in order to generalize to a multiaxial context as needed in the manufacturing simulations.

## 2. Material and deformation mechanisms

Ti-6Al-4V is a two-phase alloy containing 6 wt% Al which stabilizes the $\alpha$ phase (HCP) and 4 wt% V which stabilizes the $\beta$ phase (BCC). The proportion of these alloying elements gives attractive mechanical properties to the material. The presence of Al inhibits twinning, even though it is a common deformation mechanism for HCP materials (Majorell et al., 2002). The two phases in the alloy have different properties given by their structures, with $\alpha$ exhibiting greater strength yet lower ductility and formability compared to $\beta$ phase (Tiley, 2002). The microstructure at equilibrium in room temperature consists mainly of $\alpha$ phase ($\approx 95\%$) with some retained $\beta$ phase. At around 890 °C, the $\alpha$ phase transforms to $\beta$. This temperature ($\beta$-transus) depends on the composition of Al and V. Plastic deformation occurs in $\alpha$ phase primarly through dislocation slip with a-type burgers vector. These dislocations are emitted from $\alpha - \beta$ interfaces and glide in basal planes rather than on prismatic planes because of its compatiblity with the HCP-BCC interface (Salem and Semiatin, 2009).

The material used in this work was supplied as 12 mm thick plates by ATI Allvac®, USA. It has been checked for defects using ultrasonic technique and has undergone annealing heat treatment for 6 h at 790 °C. The material is free from the hard and brittle $\alpha$-case (oxygen-rich surface layer). Microscopic examination of the received material revealed a bi-modal structure with primary alpha surrounded by transformed beta (Widmanstätten structure). When heated to elevated temperature followed by slow cooling, both globular and lamellar grains demonstrated coarsening.

Cylindrical specimens machined from the plates were used in the experiments. The axis of the specimens is oriented in the transverse direction of rolling. Mechanical properties of Ti-6Al-4V depend on different parameters like thermo-mechanical processing, chemical composition, interstitial impurities, etc. The chemical composition of the material is shown in Table 1.

**Table 1**
Chemical composition given in wt.%. Remaining is Ti.

| Al | V | O | Fe | C | Si | Mn | H |
|---|---|---|---|---|---|---|---|
| 6.19 | 3.98 | 0.162 | 0.21 | 0.01 | <0.01 | <0.01 | 0.0082 |

Conrad (1981) studied the influence of various factors like solutes, interstitials, strain, strain rate, temperature, etc., on the strength and ductility of titanium systems and proposed a binary additive relationship for its yield strength. He identified the underlying mechanism of plastic flow to be glide and climb, which is assisted by diffusion. The mechanism of diffusion in Ti systems is less understood. The published diffusion data shows large scatter, which is attributed to the variation in measurement techniques (Liu and Welsch, 1988; Mishin and Herzig, 2000). Semiatin et al. (2003) measured the diffusivity of Al and V in $\beta$-Ti between 700 and 950 °C. It has been reported that dislocations in Ti-6Al-4V act as high-diffusivity paths leading to an enhanced diffusion (Park et al., 2008a). Globularization of Ti-6Al-4V alloy at elevated temperature is reported by many authors (Stefansson and Semiatin, 2003; Semiatin et al., 2005; Yeom et al., 2007; Zhao et al., 2007; Sargent et al., 2008; Park et al., 2008b). Bai et al., 2012, based on experimental evidence, demonstrated the mechanism of globularization and how it leads to flow softening. This can also result in stress relaxation.

## 3. Formulation of the flow stress model

The flow stress model is formulated on a material volume which represents the average behavior of a large number of grains, dislocations, etc. This approach provides a bridge between various sub-micro scale phenomena and macro-scale continuum mechanics.

Plastic strain is related to motion of dislocations, while hardening or softening is associated with interaction of dislocations. With the increase of dislocation density, the dislocations themselves get entangled and prevent further motion, which results in isotropic hardening. Recovery and recrystallization are two competing restoration mechanisms and they counteract the strain hardening. In order to compute evolution of the material state, dislocation density and vacancy concentration are used as internal state variables in this model.

### 3.1. Flow stress

An incompressible von Mises model for plasticity is used here. Plastic deformation is assumed to be isotropic, although some anisotropic behavior is observed. The flow stress is assumed to consist of two parts (Seeger, 1956; Bergström, 1969; Kocks, 1976),

$$\sigma_y = \sigma_G + \sigma^* \tag{1}$$

where, $\sigma_G$ is the athermal stress contribution from the long-range interactions of the dislocation substructure. The second term $\sigma^*$, is the friction stress needed to move dislocations through the lattice and to pass short-range obstacles. Thermal vibrations can assist dislocations to overcome these obstacles. Many non-linear variants of Eq. (1) to model the precipitate hardening are available in the literature (Nembach and Neite, 1985). However, linear superposition is chosen here based on the behavior of Titanium alloys identified by Conrad (1981).

#### 3.1.1. Long-range stress component:

The long-range term from Eq. (1) is derived by Seeger (1956) as,

$$\sigma_G = m\alpha Gb\sqrt{\rho_i} \tag{2}$$

where $m$ is the Taylor orientation factor translating the effect of the resolved shear stress in different slip systems into effective stress and strain quantities. Furthermore, $\alpha$ is a proportionality factor, $b$ is the Burger's vector and $\rho_i$ is the immobile dislocation density. The shear modulus ($G$) can be computed from the Young's modulus ($E$) and Poisson ratio ($\nu$) as,

$$G = \frac{E}{2(1+\nu)} \tag{3}$$

#### 3.1.2. Short-range stress component:

The dislocation velocity is related to plastic strain rate via the Orowan equation (Orowan, 1948)

$$\dot{\bar{\varepsilon}}^p = \frac{\rho_m b \bar{v}}{m} \tag{4}$$

where $\bar{v}$ is the average velocity of the mobile dislocations, $\rho_m$ is the mobile dislocation density and $\dot{\bar{\varepsilon}}^p$ is the plastic strain rate. This velocity is related to the time taken by a dislocation to pass an obstacle, most of which is the waiting time. The velocity is written according to Frost and Ashby (1982) as,

$$\bar{v} = \lambda v_a e^{-\Delta G/kT} \tag{5}$$

where $\lambda$ is the average obstacle spacing, $v_a$ is the attempt frequency, $\Delta G$ is the activation energy, $k$ is the Boltzmann constant and $T$ is the temperature in Kelvin. Here, $e^{-\Delta G/kT}$ can be considered as the probability that the activation energy is supplied locally. Substituting for velocity, Eq. (4) can be written as,

$$\dot{\bar{\varepsilon}}^p = f e^{-\Delta G/kT} \tag{6}$$

where the form of the function $f$ and $\Delta G$ depend on the applied stress, strength of obstacles, etc., (Frost and Ashby, 1982). The stress available to move a dislocation past an obstacle is the difference between applied stress and the long-range flow stress component. Since the equivalent stress during plastic deformation is equal to the flow stress, $f = f(\bar{\sigma} - \sigma_G) = f(\sigma^*)$. The activation energy for dislocation motion can be written according to Kocks et al. (1975) as,

$$\Delta G = \Delta F\left[1 - \left(\frac{\sigma^*}{\sigma_{ath}}\right)^p\right]^q, \quad 0 \leqslant p \leqslant 1,\ 1 \leqslant q \leqslant 2 \tag{7}$$

Here, $\Delta F = \Delta f_0 G b^3$ is the activation energy necessary to overcome short-range obstacles and $\sigma_{ath} = \tau_0 G$ is the shear strength in the absence of thermal energy. Some guidelines for selection of $\Delta f_0$ and $\tau_0$ are given in Table 2. Based on the above formulation, the strain rate dependent part of the yield stress in Eq. (1) can be derived according to the Kocks–Mecking formulation (Kocks et al., 1975; Mecking and Kocks, 1981) as,

$$\sigma^* = \tau_0 G\left[1 - \left[\frac{kT}{\Delta f_0 G b^3}\ln\left(\frac{\dot{\varepsilon}^{ref}}{\dot{\bar{\varepsilon}}^p}\right)\right]^{1/q}\right]^{1/p} \tag{8}$$

Here, $\dot{\varepsilon}^{ref}$ is the reference strain rate.

### 3.2. Evolution of immobile dislocation density

The basic components for the yield stress in Eq. (1) are obtained from Eqs. (2) and (8). However, the evolution of $\rho_i$ in Eq. (2) needs to be computed. The model for evolution of the immobile dislocation density has two parts: hardening and restoration.

$$\dot{\rho}_i = \dot{\rho}_i^{(+)} - \dot{\rho}_i^{(-)} \tag{9}$$

#### 3.2.1. Hardening process

It is assumed that mobile dislocations move, on average, a distance $\Lambda$ (mean free path), before they are immobilized or annihilated. According to the Orowan equation (Orowan, 1948), density of mobile dislocations and their average velocity are proportional to the plastic strain rate. It is reasonable to assume that increase in immobile dislocation density also follows the same relation (Mecking and Kocks, 1981). This leads to,

$$\dot{\rho}_i^{(+)} = \frac{m}{b}\frac{1}{\Lambda}\dot{\bar{\varepsilon}}^p \tag{10}$$

where $m$ is the Taylor orientation factor. The mean free path can be computed from the grain size ($g$) and dislocation subcell or subgrain diameter ($s$) as,

$$\frac{1}{\Lambda} = \left(\frac{1}{g} + \frac{1}{s} + others\right) \tag{11}$$

where *others* denote contributions from obstacles like precipitates, interstitial elements, martensite lathes, etc. Models for recrystallization, grain growth, precipitation, dissolution, etc., can be included here (Fisk, 2011).

The formation and evolution of subcells has been modeled using a relation proposed by Holt (1970).

$$s = K_c\frac{1}{\sqrt{\rho_i}} \tag{12}$$

The model for grain growth based on isothermal measurements can be written according to Porter and Easterling (1992) and Sargent et al. (2008) as,

$$g^n - g_0^n = Kt \tag{13}$$

Here, $g_0$ is the original grain size, $t$ is the time elapsed and $K$ is the calibration parameter.

**Table 2**
Activation energy factor and shear strength of different obstacles from Frost and Ashby, 1982 ($l$ is the mean spacing of the obstacles).

| Obstacle strength | $\Delta f_0$ | $\tau_0$ | Example |
|---|---|---|---|
| Strong | 2 | $> \frac{b}{l}$ | Strong precipitates |
| Medium | 0.2 – 1.0 | $\approx \frac{b}{l}$ | Weak precipitates |
| Weak | $< 0.2$ | $\ll \frac{b}{l}$ | Lattice Resistance, |

*3.2.2. Restoration processes*

Annihilation and remobilization of dislocations are thermally activated reorganization processes that lead to restoration of the deformed lattice (Roberts and Bergström, 1973). In high-stacking fault materials, recovery process might balance the effects of strain hardening leading to a constant flow stress.

The model for recovery by glide can be written based on the formulation by Bergström (1983) as,

$$\dot{\rho}_i^{(-)} = \Omega \rho_i \dot{\bar{\varepsilon}}^p \tag{14}$$

where $\Omega$ is a function dependent on temperature. This is analogous to the model by Kocks et al. (1975) as $\rho_i$ and $\dot{\bar{\varepsilon}}^p$ are proportional to $\rho_m$ and $\bar{v}$, respectively.

The motion of dislocations perpendicular to its glide plane is called climb, which reduces the density of the immobile dislocations. In addition to dislocations, vacancies are also created during plastic deformation (Friedel, 1964). This has significant effect on diffusion controlled processes such as climb and dynamic strain aging. Militzer et al. (1994) proposed a model for climb based on Sandstrom and Lagneborg (1975) and Mecking and Estrin (1980). According to Lindgren et al. (2008), the recovery due to climb is enhanced by the increase in diffusivity from excess vacancy concentration. This is written as

$$\dot{\rho}_i^{(-)} = 2c_\gamma D_{app} \frac{Gb^3}{kT} \left(\rho_i^2 - \rho_{eq}^2\right) \tag{15}$$

where $c_\gamma$ is a material coefficient and $D_{app}$ is the apparent diffusivity of the material. Lindgren et al. (2008) used the lattice diffusion enhanced by excess vacancies given in equation (24) as $D_{app}$. It is further developed in this work to include the effects of phase transformation and pipe diffusion (see Eq. 27).

Sargent et al., 2008 have observed that, in Ti-6Al-4V, static and dynamic coarsening occur at elevated temperatures (650–815 °C) and dynamic coarsening occurs at a faster rate as compared to the static. The deformation energy stored as dislocations and the supplied thermal energy provide the driving force for this grain growth. Coarsening also results in the grain becoming more globular; hence, it is called globularization. During coarsening, grain boundaries move through the lattice and annihilate the dislocations, thereby resulting in a reduction of the dislocation density (Jessell et al., 2003). Thus, globularization reduces the flow stress of the material. A model for the evolution of dislocation density during recrystallization is proposed by Pietrzyk and Jedrzejewski (2001), Montheillet and Jonas (2009). Since the underlying mechanisms of recrystallization and globularization are similar, this model can be adapted here as shown below.

$$\text{if} \quad \rho_i \geqslant \rho_{cr}$$
$$\dot{\rho}_i^{(-)} = \psi \dot{X}_g \left(\rho_i - \rho_{eq}\right); \ \text{until} \ \ \rho_i \leqslant \rho_{eq} \tag{16}$$
$$\text{else}$$
$$\dot{\rho}_i^{(-)} = 0 \tag{17}$$

Here, $\rho_{cr}$ is the critical dislocation density above which globularization is initiated, $\rho_{eq}$ is the equilibrium value of dislocation density, $\dot{X}_g$ is the globularization rate and $\psi$ is a calibration constant. According to this model, the effect of grain growth on the reduction of flow stress is included only when the stored deformation energy is sufficiently high. This is expressed through the criterion $\rho_i \geqslant \rho_{cr}$.

The mechanism of globularization of Ti-6Al-4V has been studied by Stefansson and Semiatin (2003). They observed that during deformation and shortly after wards, globularization is driven by dislocation substructure resulting in boundary splitting and edge spheroidization. This is followed by a second stage characterized by grain coarsening. This is similar to the two-stage process of dynamic and static recrystallization modeled by Thomas and Semiatin (2006). Based on their formulation, globularization is modeled as,

$$X_g = X_d + (1 - X_d) X_s \tag{18}$$

Here, the volume fractions $X_g, X_d$ and $X_s$ denote total globularized, its dynamic component and static component, respectively. Pietrzyk and Jedrzejewski (2001) proposed a model for static recrystallization. Also, a model for grain growth during recrystallization is proposed by Montheillet and Jonas (2009). Assuming that grain growth and static recrystallization have the same driving force, static globularization rate can be written as,

$$\dot{X}_s = M \frac{\dot{g}}{g} \tag{19}$$

where, $M$ is a material parameter. The rate of dynamic globularization is modeled based on Thomas and Semiatin (2006) as,

$$\dot{X}_d = \frac{-Bk\dot{\bar{\varepsilon}}^p}{\left(\bar{\varepsilon}^p\right)^{k+1} e^{B\left(\bar{\varepsilon}^p\right)^{-k}}} \tag{20}$$

where, $B$ and $k$ are material parameters. Eqs. (18)–(20) for computing the globularization fraction are used only when condition $\rho_i \geqslant \rho_{cr}$ for Eq. (16) is satisfied.

### 3.3. Self diffusion enhanced by excess vacancies and dislocations

Diffusion occurs by the motion of defects like vacancies and interstitial atoms and by atomic exchange. But vacancy motion is the predominant diffusion mechanism, due to the lower activation energy of vacancy migration (Friedel, 1964). The self diffusion coefficient can be written according to Reed-Hill and Abbaschian (1991) as,

$$D_v = a^2 \nu e^{\frac{\Delta S_{vm}+\Delta S_{vf}}{k}} e^{-\frac{Q_{vm}+Q_{vf}}{kT}} = D_{l0} e^{-\frac{Q_v}{kT}} \tag{21}$$

where, $a$ is the lattice constant, $\nu$ is the lattice vibration frequency, $\Delta S_{vm}$ is the entropy increase due to the motion of a vacancy, $Q_{vm}$ is the energy barrier to be overcome for vacancy motion and $D_{l0}$ is the activity factor of lattice diffusion.

Vacancy migration leads to vacancy annihilation and it follows an Arrhenius-type relation as below.

$$D_{vm} = a^2 \nu e^{\frac{\Delta S_{vm}}{k}} e^{-\frac{Q_{vm}}{kT}} \tag{22}$$

Introducing the equilibrium concentration of vacancy from Eq. (28), self-diffusivity can be written as,

$$D_v = c_v^{eq} D_{vm} \tag{23}$$

Thus the self-diffusivity is the product of vacancy diffusivity and its equilibrium concentration. This can be rewritten generically for any concentration of vacancy as,

$$D_l^* = \frac{c_v}{c_v^{eq}} D_v \tag{24}$$

Lattice diffusivity of $\alpha$ and $\beta$ phases differ by many order of magnitude, which results in a jump at the $\beta$-transus temperature (Mishin and Herzig, 2000). This transition is modeled by scaling the diffusivity with the volume fraction of each phase.

$$D_l = \frac{c_v}{c_v^{eq}} \left[ D_\alpha \cdot (1-f)^w + D_\beta \cdot f^w \right] = \frac{c_v}{c_v^{eq}} D_v^* \tag{25}$$

where $f = f(T)$ is the volume fraction of $\beta$ phase. The effect of phase change on vacancy concentration is ignored here.

Lattice diffusion is responsible for climb at high temperatures. However, at intermediate temperatures, diffusion along dislocation lines, referred to as core or pipe diffusion, has a larger effect on climb (Prinz et al., 1982). While studying the static grain growth of fine-grained Ti-6Al-4V, Johnson et al. (1998) concluded that grain boundary and pipe diffusion are the controlling mechanisms at temperatures less than $0.5T_{melt}$. The effect of grain boundary diffusion can be neglected in the proposed model because of the larger grain size of the material considered. Reed-Hill and Abbaschian (1991) proposed an Arrhenius-type equation for grain boundary diffusion similar to Eq. (22). Since the basic mechanisms of grain boundary and dislocation core diffusion are the same (Shewmon, 1963), a similar formulation can be employed here.

$$D_p = D_{p0} e^{-\frac{Q_p}{kT}} \tag{26}$$

where, $D_{p0}$ is the frequency factor and $Q_p$ is the activation energy.

The total diffusive flux in the material is enhanced by the short circuit diffusion, which is dependent on the relative cross sectional area of pipe and matrix, parameter $N$ in Eq. (27). According to the model proposed by Porter and Easterling (1992), Militzer et al. (1994), the apparent diffusivity can be written as

$$\begin{aligned} D_{app} &= D_l + N D_p \\ N &= \frac{n_a^p n_\rho}{N_a^l} \end{aligned} \tag{27}$$

where, $n_a^p$ is the number of atoms that can fill the cross-sectional area of a dislocation, $n_\rho$ is the number of dislocations intersecting a unit area ($= \rho_i$) and $N_a^l$ is the number of atoms per unit area of lattice.

### 3.4. Evolution of excess vacancy concentration

When subjected to deformation or temperature change, materials generate excess vacancies. Creation of vacancy increases entropy, but consumes energy, and its concentration increases with temperature and deformation. The concentration of vacancies attain equilibrium if left undisturbed in isothermal conditions. The model considered here is only concerned with mono-vacancies. The equilibrium concentration of vacancies at a given temperature, according to Reed-Hill and Abbaschian (1991), Cahn and Peter (1996), is

$$c_v^{eq} = e^{\frac{\Delta S_{vf}}{k}} e^{-\frac{Q_{vf}}{kT}} \tag{28}$$

where, $\Delta S_{vf}$ is the increase in entropy while creating a vacancy and $Q_{vf}$ is the activation energy for vacancy formation.

Militzer et al. (1994) proposed a model for excess vacancy concentration with generation and annihilation components as

$$\dot{c}_v^{ex} = \dot{c}_v - \dot{c}_v^{eq} = \left[ \chi \frac{\sigma b}{Q_{vf}} + \zeta \frac{c_j}{4b^2} \right] \frac{\Omega_0}{b} \dot{\bar{\varepsilon}} - D_{vm} \left[ \frac{1}{s^2} + \frac{1}{g^2} \right] (c_v - c_v^{eq}) \tag{29}$$

Here, $\chi = 0.1$ is the fraction of mechanical energy spent on vacancy generation, $\Omega_0$ is the atomic volume and $\zeta$ is the neutralization effect by vacancy emitting and absorbing jogs, as computed as below.

$$\zeta = \begin{cases} 0.5 - \zeta_0 c_j & \text{if } c_j \leqslant 0.5/\zeta_0, \\ 0 & \text{if } c_j > 0.5/\zeta_0, \end{cases} \quad \zeta_0 = 10 \tag{30}$$

The concentration of jogs is given as

$$c_j = e^{-\frac{Q_{jf}}{kT}}; \quad Q_{jf} = \frac{Gb^3}{4\pi(1-\nu)}$$

where $Q_{jf}$ is the activation energy of jog formation.

Assuming that only long-range stress contributes to vacancy formation and adding the contribution from temperature change, Eq. (29) becomes

$$\dot{c}_v^{ex} = \left[\chi \frac{m\alpha G b^2 \sqrt{\rho_i}}{Q_{vf}} + \zeta \frac{c_j}{4b^2}\right] \frac{\Omega_0}{b} \dot{\bar{\varepsilon}} - D_{vm}\left[\frac{1}{s^2} + \frac{1}{g^2}\right](c_v - c_v^{eq}) + c_v^{eq}\left(\frac{Q_{vf}}{kT^2}\right)\dot{T} \tag{31}$$

## 4. Stress-update

To compute the flow stress evolution for arbitrary paths, a radial return algorithm can be used (Simo and Taylor, 1986; Simo and Hughes, 1998). This requires hardening modulus and updated internal variables for each time increment. In the proposed model, $\sigma_y = \sigma_y(\bar{\varepsilon}^p, \rho_i, c_v)$ where $\rho_i$ and $c_v$ are described by a coupled set of differential equations. These internal variables can be written in vector form as $\mathbf{q}^T = [q_1, q_2] = [\rho_i, c_v]$. An implicit iterative procedure is used in every time increment to calculate its evolution. Assuming a constant $\dot{\bar{\varepsilon}}^p$ during the increment, the change in state variables can be computed as

$$\mathbf{H}^T = [H_1, H_2] = 0 \tag{32}$$

$$H_1 = \Delta q_1 - \left[\frac{m}{b\Lambda}\Delta\bar{\varepsilon}^p - \Omega q_1 \Delta\bar{\varepsilon}^p - 2c_\gamma\left(\frac{D_v^*}{c_v^{eq}} q_2 + \frac{n_a^p}{N_a^l} q_1\right)\frac{Gb^3}{kT}\left(q_1^2 - \rho_{eq}^2\right)\rho_{i0}\Delta t - \psi X_g\left(q_1 - \rho_{eq}\right)\right] \tag{33}$$

$$H_2 = \Delta q_2 - \left[\chi \frac{\Omega_0 m\alpha G b}{Q_{vf}}\sqrt{q_1}\Delta\bar{\varepsilon}^p + \zeta\frac{c_j\Omega_0}{4b^3}\Delta\bar{\varepsilon}^p - D_{vm}\left[\frac{1}{s^2} + \frac{1}{g^2}\right](q_2 - c_v^{eq})\Delta t + c_v^{eq}\left(\frac{Q_{vf}}{kT^2}\right)\Delta T\right] \tag{34}$$

The iterative change in $\mathbf{q}$ can be written as

$$d\mathbf{q} = -\left[\frac{\partial \mathbf{H}_{(i)}}{\partial \mathbf{q}}\right]^{-1} \mathbf{H}_{(i)} \tag{35}$$

where, $i$ is the iteration counter. The value of the state variables can be updated as

$$\mathbf{q}_{(i+1)} = \mathbf{q}_{(i)} + d\mathbf{q} \tag{36}$$

The hardening modulus needed in the radial return algorithm is

$$H' = \frac{d\sigma_y(\mathbf{q})}{d\bar{\varepsilon}^p} = \frac{\partial\sigma_y}{\partial\mathbf{q}}\frac{\partial\mathbf{q}}{\partial\bar{\varepsilon}^p} = \frac{\partial\sigma_G}{\partial\rho_i}\left[\frac{\partial\rho_i}{\partial\bar{\varepsilon}^p} + \frac{\partial\rho_i}{\partial c_v}\frac{\partial c_v}{\partial\bar{\varepsilon}^p}\right] + \frac{\partial\sigma^*}{\partial\bar{\varepsilon}^p} \tag{37}$$

The model for grain growth given in Eq. (13) can be written in incremental form as

$$g_{i+1} = \sqrt[n]{g_i^n + K\Delta t} \tag{38}$$

## 5. Experiments

Compression tests performed at the nominal temperatures 20, 100, 200, 300, 400, 500, 600, 700, 800, 900, 950, 1000 1050 and 1100 °C and strain rates from 0.001 $s^{-1}$ to 1.0 $s^{-1}$ were used to calibrate the model. The length (L≈8 mm) and diameter (D) of the specimens are varied ($1.2 \leqslant \frac{L}{D} \leqslant 1.4$) for each temperature to receive a measurable force response from the Gleeble® thermo-mechanical simulator and to prevent buckling. In order to reduce the friction between the specimen and anvil, Tantalum films were placed between the two. In-spite of this, some specimens exhibited barreling, which is evidence of significant friction. The specimens are heated to test temperature at a rate of 10 °C$s^{-1}$. It is held for 30 s to achieve an even temperature distribution followed by compression at a given strain rate.

During compression, strain rate and temperature are controlled using a closed loop control system and force is measured from the load cells attached to the anvils. Temperature is increased to the predefined value by using resistance electrical heating. However, due to the additional deformation heating, the temperature of the specimen increases (<50 °C for $\dot{\bar{\varepsilon}} = 1\ s^{-1}$ and <5 °C for $\dot{\bar{\varepsilon}} = 0.001\ s^{-1}$) during deformation. This is recorded with the thermocouple welded to the specimen

and used in the model calibration. Diametrical change of the specimen is measured during the tests. This data combined with the force measurement from the load cell is used to compute the stress. The data obtained from measurement is smoothed to remove the noise generated by the dynamics of the machine operation. Corrections are made to compensate for the compliance of the anvil and lubricant film. Owing to the strong affinity of the alloy to oxygen at high temperatures, the experiments were performed in an evacuated chamber.

## 6. Optimization of the model

The parameters for the model are obtained by calibration using an in-house Matlab®-based toolbox. This toolbox uses Matlab®'s constrained minimization routine and can handle multiple experiments for optimization (Domkin et al., 2003).

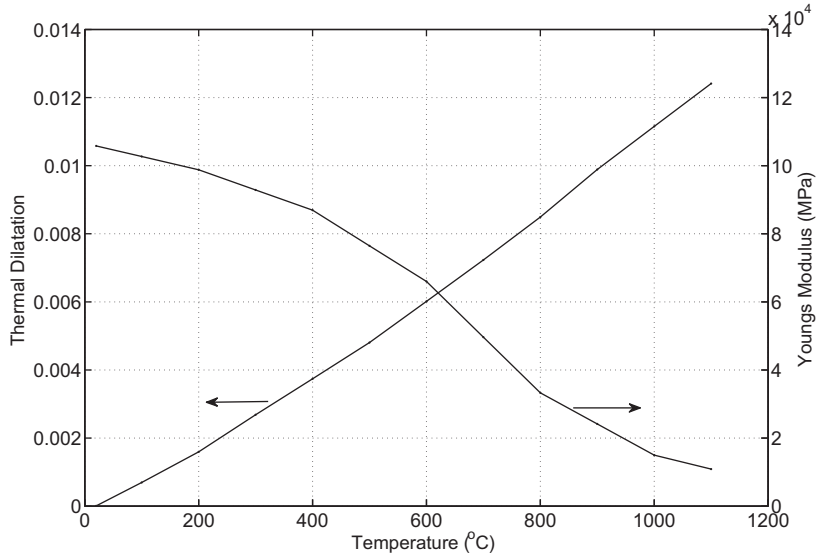


**Fig. 1.** Thermal dilatation ($\varepsilon_{th}$) and Young's modulus.

**Table 3**
Constant parameters for the model.

| Parameter | Dimension | Value | Reference |
|---|---|---|---|
| $T_{melt}$ | ° C | 1600 | f |
| $T_{\beta-transus}$ | ° C | 890 | f |
| $k$ | $JK^{-1}$ | $1.38 \cdot 10^{-23}$ | f |
| $b$ | m | $2.95 \cdot 10^{-10}$ | a |
| $D_{\alpha 0}$ | $m^2s^{-1}$ | $5 \cdot 10^{-6}$ | d |
| $D_{\beta 0}$ | $m^2s^{-1}$ | $3 \cdot 10^{-7}$ | d |
| $Q_{vf}$ | J | $1.9 \cdot 10^{-19}$ | b |
| $Q_{vm}$ | J | $2.49 \cdot 10^{-19}$ | a |
| $Q_{\beta}$ | J | $2.5 \cdot 10^{-19}$ | d |
| $Q_p$ | J | $1.61 \cdot 10^{-19}$ | a |
| $n_a^p$ | – | 2 | f |
| $n_\rho$ | – | $\rho_i$ | f |
| $\Omega_0$ | $m^3$ | $1.76 \cdot 10^{-29}$ | a |
| $g_0$ | m | $2 \cdot 10^{-6}$ | f |
| $K$ | $m^3hr$ | $5 \cdot 10^{-18}$ | e |
| $n$ | – | 3 | e |
| $\dot{\varepsilon}_{ref}$ | $s^{-1}$ | $10^6$ | a |
| $\Delta S_{vm}$ | $JK^{-1}$ | $1.38 \cdot 10^{-23}$ | g |

[a]Frost and Ashby (1982).
[b]Novikov et al. (1980).
[c]Conrad (1981).
[d]Mishin and Herzig (2000).
[e]Sargent et al. (2008).
[f]Calculated or measured value.
[g]Hernan et al. (2005).

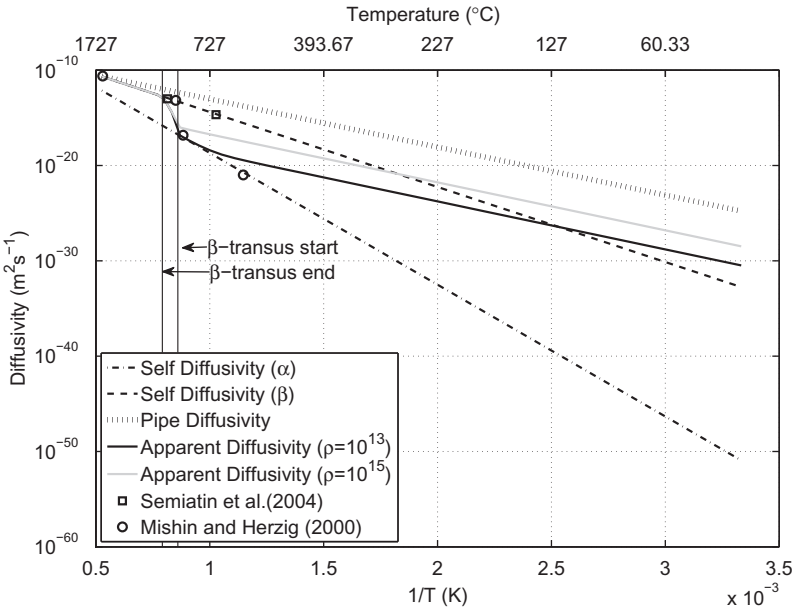


**Fig. 2.** Self diffusion.

**Table 4**
Calibrated parameters of the model.

| Parameter | Dimension | Value |
|---|---|---|
| $D_{p0}$ | $m^2s^{-1}$ | $10^{-8}$ |
| $N_a^l$ | – | $10^{19}$ |
| $p$ | – | 0.3 |
| $q$ | – | 1.8 |
| $\Omega$ | – | 38 |
| $\rho_{eq}$ | $m^{-2}$ | $10^{10}$ |

**Table 5**
Calibrated temperature-dependant parameters of the model.

| T [° C] | 25 | 100 | 200 | 300 | 400 | 500 | 600 | 700 | 800 | 900 | 1000 | 1100 |
|---|---|---|---|---|---|---|---|---|---|---|---|---|
| $\alpha$ | 2.30 | 1.92 | 1.90 | 1.90 | 2.10 | 2.15 | 1.70 | 0.80 | 1.00 | 1.15 | 1.20 | 1.10 |
| $C_\gamma$ $[10^{-1}]$ | 0.00 | 0.00 | 0.00 | 0.00 | 0.00 | 3.00 | 4.00 | 5.00 | 5.00 | 0.50 | 1.00 | 2.00 |
| $K_c$ $[10^2]$ | 0.40 | 0.40 | 0.40 | 0.40 | 0.40 | 0.40 | 0.40 | 0.80 | 1.20 | 1.20 | 1.20 | 1.20 |
| $\tau_0$ $[10^{-1}]$ | 0.10 | 0.20 | 0.20 | 0.20 | 0.20 | 0.40 | 1.20 | 1.50 | 3.50 | 3.00 | 1.00 | 0.50 |
| $\Delta f_0$ | 0.50 | 0.50 | 0.50 | 0.50 | 0.50 | 0.60 | 0.80 | 1.70 | 1.70 | 1.55 | 1.30 | 0.90 |
| $\rho_i^{init}$ $[10^{14}]$ | 1.00 | 1.00 | 1.00 | 1.00 | 1.00 | 1.00 | 0.70 | 0.10 | 0.10 | 0.10 | 0.01 | 0.01 |
| $\rho_i^{crit}$ $[10^{14}]$ | 5.00 | 5.00 | 5.00 | 5.00 | 2.24 | 2.00 | 1.50 | 0.20 | 0.20 | 0.20 | 0.10 | 0.10 |
| $B$ | 1.00 | 1.00 | 1.00 | 1.00 | 0.50 | 0.50 | 0.50 | 0.60 | 0.50 | 0.10 | 0.01 | 0.01 |
| $k$ | 2.00 | 2.00 | 2.00 | 2.00 | 2.00 | 2.00 | 1.00 | 1.50 | 2.00 | 2.00 | 2.00 | 2.00 |
| $M$ $[10^2]$ | 0.00 | 0.00 | 0.00 | 0.00 | 0.00 | 1.00 | 6.00 | 6.00 | 1.00 | 1.00 | 1.00 | 1.00 |
| $\psi$ | 0.00 | 0.00 | 0.00 | 0.00 | 0.05 | 0.05 | 0.60 | 2.00 | 8.00 | 1.00 | 1.00 | 1.00 |
| $K$ $[10^{-1}]$ | 0.00 | 0.00 | 0.00 | 0.00 | 0.00 | 0.05 | 0.25 | 6.50 | 8.00 | 8.00 | 8.00 | 8.00 |

The shear modulus is computed according to equation (3) using the temperature-dependent Young's modulus given in Fig. 1. These values are obtained from isothermal tension tests using 0.2% offset. The Poisson ratio is assumed to be 0.33 for all temperatures (Cai et al., 2011). Strain has contributions from mechanical and thermal loads. Fig. 1 shows the thermal strain measured using a differential expansion dilatometer. According to Hernan et al. (2005), the entropy of vacancy migration for HCP metals lies in the range (0.9–1.6) k. Here, $\Delta S_{vm}$ is assumed to be equal to $k$. The activation energy of vacancy formation

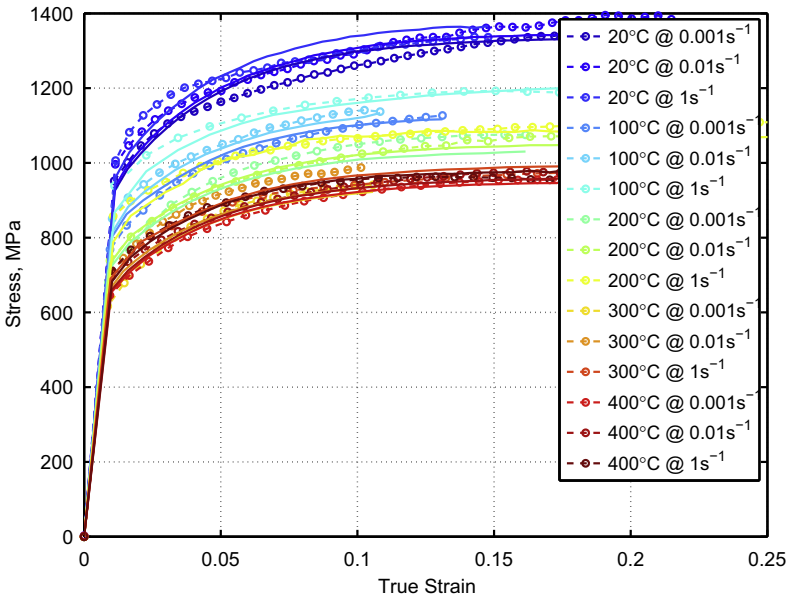


**Fig. 3.** Measured and computed stress–strain curve for 20 °C to 400 °C.

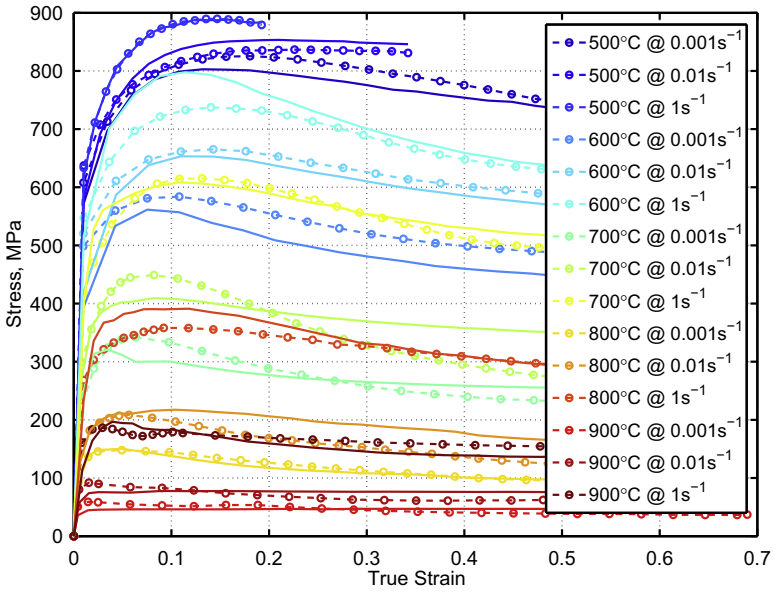


**Fig. 4.** Measured and computed stress–strain curve for 500 °C to 900 °C.

($Q_{vf}$) measured by Novikov et al. (1980) for pure Ti is used in this work. Table 3 lists the various material constants obtained from measurements and literature.

Conrad, 1981 measured the dislocation density of undeformed Ti alloy with (0.1–1.0) at.% $O_{eq}$ to be of the order of $10^{13}$ m$^{-2}$. Picu and Majorell (2002) used $\rho_{init} = 10^{12}$ m$^{-2}$ based on calibration. Following a similar approach, varying values of $\rho_i^{init}$ between ($10^{14} - 10^{12}$ m$^{-2}$) for increasing temperature are used here.

Fig. 2 shows diffusivities needed to compute the apparent diffusivity of Ti-6Al-4V for different values of dislocation density which correspond to annealed and deformed material. Enhanced diffusivity due to pipe diffusion has a significant effect at low temperature ($< 0.5T_{melt}$). At high temperature, it is the lattice diffusivity which has significance. The measurements of Mishin and Herzig (2000) show the self diffusion of Ti in $\alpha$ and $\beta$ phases, whereas the measurement of Semiatin et al. (2003) show diffusion of Al in $\beta$ phase of Ti-6Al-4V. The activity factor of pipe diffusion ($D_{p0}$) is assumed to be of the same order as that of lattice diffusion.

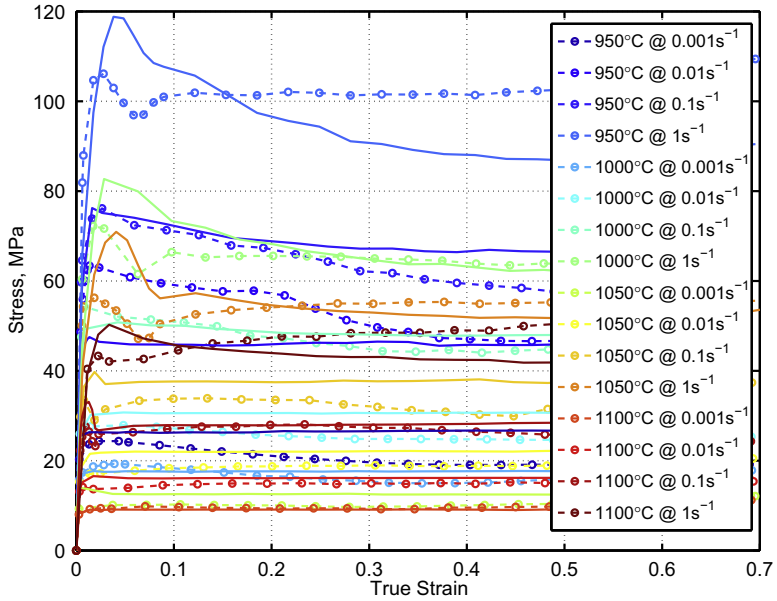


**Fig. 5.** Measured and computed stress–strain curve for 950 °C to 1100 °C.

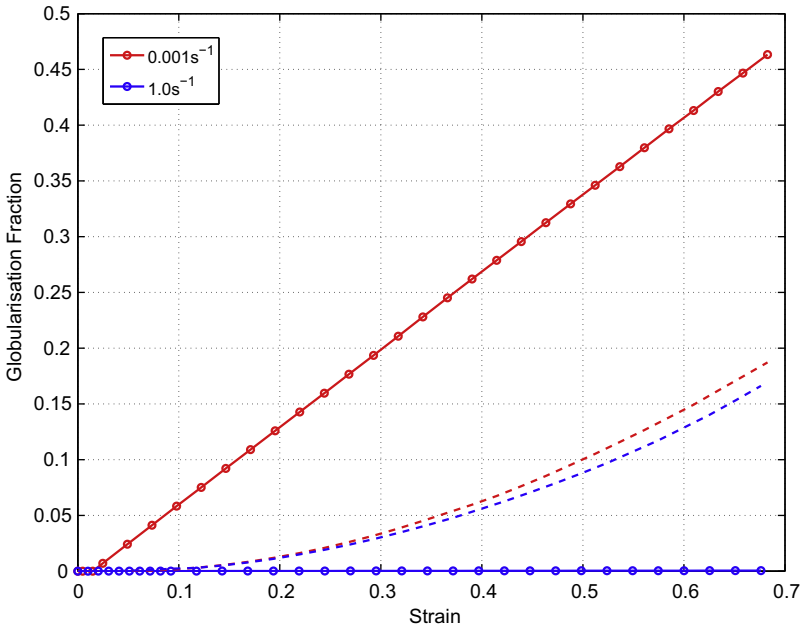


**Fig. 6.** Globularization during deformation at 800 °C.

The different parameters of the model obtained after calibration using $\sigma$-$\varepsilon$ measurements are shown in Tables 4 and 5.

## 7. Comparison of model and experiments

Measured and computed stress–strain curves are plotted in Figs. 3–5. The dotted lines with markers denote measurements and continuous lines denote simulations. Compression tests performed at 20 °C to 400 °C showed very little rate dependence and resulted in hardening followed by fracture. Here, dislocation glide is the dominant deformation mechanism. Tests performed between 500 °C to 900 °C resulted in flow softening after the initial hardening. Sargent et al. (2008) observed that grain coarsening is enhanced approximately one order of magnitude during deformation as compared to static

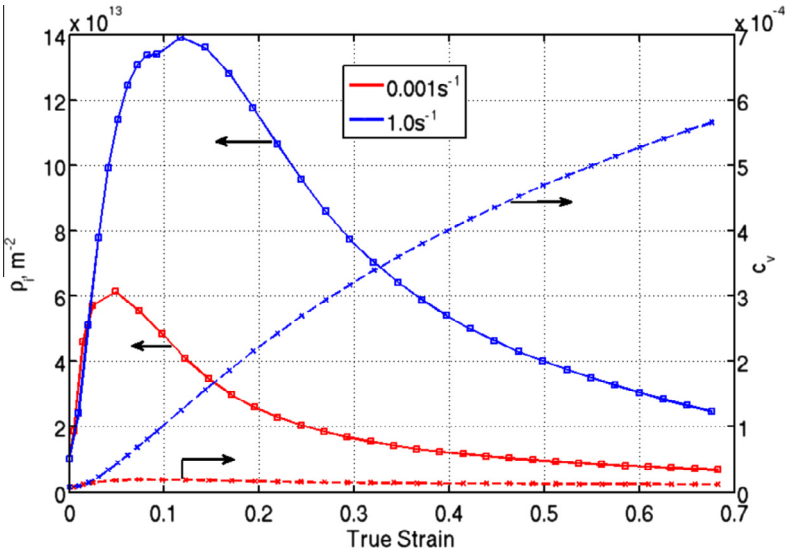


**Fig. 7.** Evolution of dislocation density and excess vacancy concentration during deformation at 800 °C.

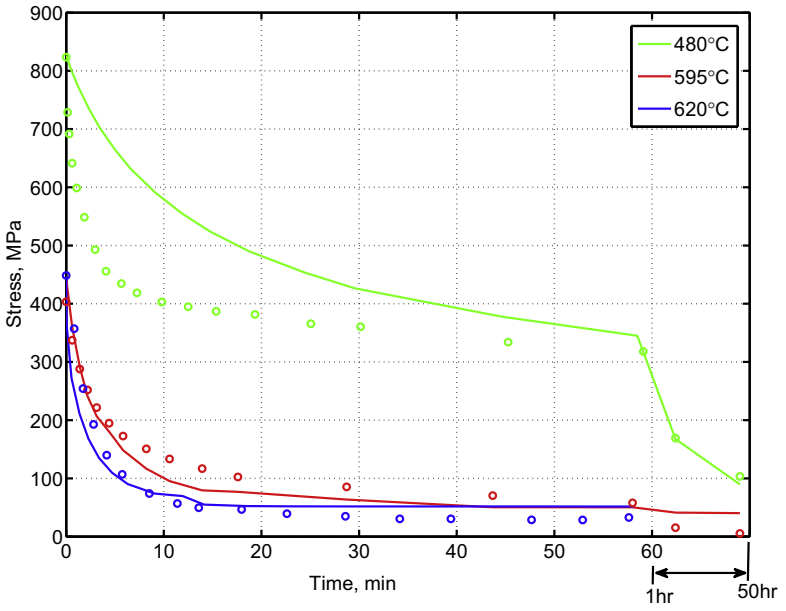


**Fig. 8.** Measured and computed stress relaxation at 480 °C, 595 °C and 620 °C.

conditions. Dynamic globularization leads to flow softening at elevated temperatures (Yeom et al., 2007). In addition, dislocation glide and climb are also dominant during this temperature range. Comparing the theoretical and experimental results in Figs. 3–5 shows that the model can reproduce the dominant phenomena observed during the plastic deformation of Ti-6Al-4V. Fig. 6 shows the globularization kinetics during deformation at 800 °C with dotted lines showing dynamic component and continuous lines showing static component. Red lines[1] denote deformation at 0.001 $s^{-1}$ and blue at 1 $s^{-1}$. Dislocation density and excess vacancy concentration for the same tests are given in Fig. 7.

The tests from 950 °C to 1100 °C showed elastic-perfectly-plastic behavior, since the strain hardening and restoration processes are in balance.

Comparison of stress relaxation measurements done by Donachie (1988) and the model predictions are given in Fig. 8. However, the exact initial loading in the experiments and the composition of the alloy are not known. This comparison demonstrates the capacity of the model to compute the decay of stress with time.

[1] For interpretation of color in Figs. 6, the reader is referred to the web version of this article.

## 8. Discussions and conclusions

Banerjee and Williams (2013) identified a lack of physically based models for globularization of Titanium alloys. In this article, a constitutive model for Ti-6Al-4V including globularization and its effect on flow softening and stress relaxation has been developed. This model is capable of describing the plastic flow of the alloy in a wide range of temperature and strain rates by including all the dominant deformation mechanisms. Compared to the model for $\beta$-recrystallization by Fan and Yang (2011) which assumes constant strain rate sensitivity and is applicable only at high temperature, the current model can better reproduce plastic flow and softening behavior at a range of temperatures. This is crucial in the simulation of manufacturing processes. The model has already been used for simulations of a chain of manufacturing processes including forming, welding, metal deposition and heat treatment (Tersing et al., 2012; Babu and Lundbäck, 2009). Some of the parameters used in the model are available from measurements outside the domain of classical mechanical testing. Since some of these parameters are not available for this specific alloy, the data for pure Ti has been used here. The flow stress model used here follows a clear physical framework; therefore, new deformation mechanisms can be added when needed. This model assumes that the $\alpha - \beta$ phase composition of the alloy is in equilibrium at all temperatures which is sound only for low heating or cooling rates. Work to extend this model with the effects of non-equilibrium phase transformation is already in progress.

## Acknowledgment

This work was performed with the financial support of VERDI; a project under the sixth framework program of the EU. The experiments using the Gleeble® machine were done at the Materials Engineering Laboratory, University of Oulu. Dr. Mahesh C. Somani and other staff were of great help in conducting these experiments expediently and accurately.

## References

Arsenlis, A., Parks, D.M., Becker, R., Bulatov, V.V., 2004. On the evolution of crystallographic dislocation density in non-homogeneously deforming crystals. Journal of the Mechanics and Physics of Solids 52, 1213–1246.
Babu, B., Lundbäck, A., 2009. Physically based constitutive model for Ti-6Al-4V used in the simulation of manufacturing chain. In: Onate, E., Owen, D., Suarez, B. (Eds.), Computational Plasticity X: fundamentals and applications, International Center for Numerical Methods in Engineering.
Bai, Q., Lin, J., Dean, T., Balint, D., Gao, T., Zhang, Z., 2012. Modeling of dominant softening mechanisms for Ti-6Al-4V in steady state hot forming conditions. Materials Science and Engineering: A.
Banerjee, D., Williams, J., 2013. Perspectives on titanium science and technology. Acta Materialia 61, 844–879.
Barlat, F., Gracio, J.J., Lee, M.G., Rauch, E.F., Vincze, G., 2011. An alternative to kinematic hardening in classical plasticity. International Journal of Plasticity 27, 1309–1327.
Bergström, Y., 1969. Dislocation model for the stress-strain behaviour of polycrystalline alpha-iron with special emphasis on the variation of the densities of mobile and immobile dislocations. Materials Science & Engineering 5, 193–200.
Bergström, Y., 1970. A dislocation model for the stress-strain behaviour of polycrystalline [alpha]-Fe with special emphasis on the variation of the densities of mobile and immobile dislocations. Materials Science and Engineering 5, 193–200.
Bergström, Y., 1983. The plastic deformation of metals – A dislocation model and its applicability. Reviews on Powder Metallurgy and Physical Ceramics, 79–265.
Bergström, Y., Roberts, W., 1973. The dynamical strain ageing of [alpha]-iron: effects of strain rate and nitrogen content in the Jerky-flow region. Acta Metallurgica 21, 741–745.
Beyerlein, I., Tomé, C., 2008. A dislocation-based constitutive law for pure Zr including temperature effects. International Journal of Plasticity 24, 867–895.
Busso, E.P., McClintock, F.A., 1996. A dislocation mechanics-based crystallographic model of a B2-type intermetallic alloy. International Journal of Plasticity 12, 1–28.
Cahn, R.W., Peter, H., 1996, . Physical Metallurgy, 4 ed., 1. North-Holland Publishers, Amsterdam, NL.
Cai, J., Li, F., Liu, T., Chen, B., 2011. Investigation of mechanical behavior of quenched Ti-6Al-4V alloy by microindentation. Materials Characterization 62, 287–293.
Cheong, K., Busso, E., Arsenlis, A., 2005. A study of microstructural length scale effects on the behaviour of FCC polycrystals using strain gradient concepts. International Journal of Plasticity 21, 1797–1814.
Conrad, H., 1981. Effect of interstitial solutes on the strength and ductility of titanium 26, 123.
Domkin, K., Lindgren, L.E., Segle, P., 2003. Dislocation density based models of plastic hardening and parameter identification. In: The 7th International Conference on Computational Plasticity.
Donachie, J.M.J., 1988. Titanium – A Technical Guide. ASM International.
Estrin, Y., Tóth, L., Molinari, A., Bréchet, Y., 1998. A dislocation-based model for all hardening stages in large strain deformation. Acta Materialia 46, 5509–5522.
Fan, X., Yang, H., 2011. Internal-state-variable based self-consistent constitutive modeling for hot working of two-phase titanium alloys coupling microstructure evolution. International Journal of Plasticity 27, 1833–1852.
Feaugas, X., 1999. On the origin of the tensile flow stress in the stainless steel AISI 316L at 300 K: back stress and effective stress. Acta Materialia 47, 3617–3632.
Feaugas, X., Gaudin, C., 2001. Different levels of plastic strain incompatibility during cyclic loading: in terms of dislocation density and distribution. Materials Science and Engineering: A, 382–385.
Fisk, M., 2011. Modeling of induction heat treatment in a manufacturing chain. Ph.D. thesis. Luleå University of Technology, Luleå, Sweden.
Friedel, J., 1964. Dislocations. International Series of Monographs on Solid State Physics, 3. Pergamon Press.
Frost, H.J., Ashby, M.F., 1982. Deformation-Mechanism Maps: The Plasticity and Creep of Metals and Ceramics (Paperback).
Gao, C., Zhang, L., Yan, H., 2011. A new constitutive model for HCP metals. Materials Science and Engineering: A 528, 4445–4452.
Hernan, R.D., Maria, G.L., Maria, M.A., 2005. Self-diffusion in the hexagonal structure of Zirconium and Hafnium: computer simulation studies. Materials Research 8, 431–434.
Holt, D.L., 1970. Dislocation cell formation in metals. Journal of Applied Physics 41, 3197.
Horstemeyer, M.F., Bammann, D.J., 2010. Historical review of internal state variable theory for inelasticity. International Journal of Plasticity 26, 1310–1334.
James, C.W., Lutjering, G., 2003. Titanium. Springer- Verlag.

Jessell, M.W., Kostenko, O., Jamtveit, B., 2003. The preservation potential of microstructures during static grain growth. Journal of Metamorphic Geology 21, 481–491.
Chaboche, J.L., 2008. A review of some plasticity and viscoplasticity constitutive theories. International Journal of Plasticity 24, 1642–1693.
Johnson, C.H., Richter, S.K., Hamilton, C.H., Hoyt, J.J., 1998. Static grain growth in a microduplex Ti-6Al-4V alloy. Acta Materialia 47, 23–29.
Kailas, S.V., Prasad, Y.V.R.K., Biswas, S.K., 1994. Flow Instabilities and Fracture in Ti-6Al-4V Deformed in Compression at 298-673K. Metallurgical and Materials Transactions A 25A, 2173–2179.
Karpat, Y., 2011. Temperature dependent flow softening of titanium alloy Ti6Al4V: an investigation using finite element simulation of machining. Journal of Materials Processing Technology 211, 737–749.
Khan, A.S., Yu, S., 2012. Deformation induced anisotropic responses of Ti-6Al-4V alloy. Part I: Experiments. International Journal of Plasticity 38, 1–13.
Khan, A.S., Yu, S., Liu, H., 2012. Deformation induced anisotropic responses of Ti-6Al-4V alloy. Part II: a strain rate and temperature dependent anisotropic yield criterion. International Journal of Plasticity 38, 14–26.
Kocks, U., 1976. Laws for work-hardening and low-temperature creep. Journal of Engineering Materials and Technology, Transactions of the ASME, Ser H 98, 76–85.
Kocks, U.F., 1966. A statistical theory of flow stress and work-hardening. Philosophical Magazine 13, 541–566.
Kocks, U.F., Argon, A.S., Ashby, M.F., 1975. Thermodynamics and Kinetics of Slip. Progress in Material Science, 19. Pergamon Press.
Lindgren, L.E., Domkin, K., Sofia, H., 2008. Dislocations, vacancies and solute diffusion in physical based plasticity model for AISI 316L. Mechanics of Materials 40, 907–919.
Liu, Z., Welsch, G., 1988. Literature survey on diffusivities of oxygen, aluminum, and vanadium in alpha titanium, beta titanium, and in rutile. Metallurgical and Materials Transactions A 19, 1121–1125.
Majorell, A., Srivatsa, S., Picu, R.C., 2002. Mechanical behavior of Ti-6Al-4V at high and moderate temperatures–Part I: experimental results. Materials Science and Engineering A 326, 297–305.
Mecking, H., Estrin, Y., 1980. The effect of vacancy generation on plastic deformation. Scripta Metallurgica 14, 815.
Mecking, H., Kocks, U., 1981. Kinetics of flow and strain-hardening. Acta Metallurgica 29, 1865–1875.
Militzer, M., Sun, W.P., Jonas, J.J., 1994. Modeling the effect of deformation-induced vacancies on segregation and precipitation. Acta Metallurgica et Materialia 42, 133.
Mishin, Y., Herzig, C., 2000. Diffusion in the Ti-Al system. Acta Materialia 48, 589–623.
Montheillet, F., Jonas, J.J., 2009. Fundamentals of modeling for metals processing. ASM Handbook, 22A. ASM International, Materials Park, Ohio 44073-0002, pp. 220–231.
Nemat-Nasser, S., Guo, W.G., Cheng, J.Y., 1999. Mechanical properties and deformation mechanisms of a commercially pure titanium. Acta Materialia 47, 3705.
Nembach, E., Neite, G., 1985. Precipitation hardening of superalloys by ordered Gamma prime-particles. Progress in Materials Science 29, 177–319.
Novikov, I.I., Roshchupkin, V.V., Semashko, N.A., Fordeeva, L.K., 1980. Experimental investigation of vacancy effects in pure metals. Journal of Engineering Physics and Thermophysics V39, 1316.
Orowan, E., 1948. In: Symposium on Internal Stresses in Metals and Alloys, Institute of Metals, pp. 451.
Park, C.H., Ko, Y.G., Park, J.W., Ko, Y.G., 2008a. Enhanced Superplasticity Utilizing Dynamic Globularization of Ti-6Al-4V Alloy. Materials Science and Engineering: A.
Park, C.H., Park, K.T., Shin, D.H., Lee, C.S., 2008b. Microstructural Mechanisms during Dynamic Globularization of Ti-6Al-4V Alloy. Materials Transactions 49, 2196–2200.
Peeters, B., Seefeldt, M., Teodosiu, C., Kalidindi, S., Houtte, P.V., Aernoudt, E., 2001. Work-hardening/softening behaviour of b.c.c. polycrystals during changing strain paths: I. an integrated model based on substructure and texture evolution, and its prediction of the stress–strain behaviour of an IF steel during two-stage strain paths. Acta Materialia 49, 1607–1619.
Picu, R.C., Majorell, A., 2002. Mechanical behavior of Ti-6Al-4V at high and moderate temperatures–Part II: constitutive modeling. Materials Science and Engineering A 326, 306–316.
Pietrzyk, M., Jedrzejewski, J., 2001. Identification of parameters in the history dependent constitutive model for steels. CIRP Annals – Manufacturing Technology 50, 161–164.
Porter, D.A., Easterling, K.E., 1992. Phase Transformations in Metals and Alloys, second ed. CRC Press.
Prinz, F., Argon, A.S., Moffatt, W.C., 1982. Recovery of dislocation structures in plastically deformed copper and nickel single crystals. Acta Metallurgica 30, 821–830.
Przybyla, C.P., McDowell, D.L., 2011. Simulated microstructure-sensitive extreme value probabilities for high cycle fatigue of duplex Ti-6Al-4V. International Journal of Plasticity 27, 1871–1895.
Reed-Hill, R.E., Abbaschian, R., 1991. Physical Metallurgy Principles, third ed. PWS Publishing Company.
Roberts, W., Bergström, Y., 1973. The stress-strain behaviour of single crystals and polycrystals of face-centered cubic metals–a new dislocation treatment. Acta Metallurgica 21, 457–469.
Salem, A., Semiatin, S., 2009. Anisotropy of the hot plastic deformation of Ti-6Al-4V single-colony samples. Materials Science and Engineering: A 508, 114–120.
Sandstrom, R., Lagneborg, R., 1975. A model for hot working occurring by recrystallization. Acta Metallurgica 23, 387.
Sargent, G., Zane, A., Fagin, P., Ghosh, A., Semiatin, S., 2008. Low-Temperature coarsening and plastic flow behavior of an alpha/beta titanium billet material with an ultrafine microstructure. Metallurgical and Materials Transactions A 39, 2949–2964.
Seeger, A., 1956. The mechanism of Glide and Work Hardening in FCC and HCP Metals. In: Fisher, J., Johnston, W.G., Thomson, R., Vreeland, T.J. (Eds.), Dislocations and Mechanical Properties of Crystals, pp. 243–329.
Semiatin, S., Knisley, S., Fagin, P., Barker, D., Zhang, F., 2003. Microstructure evolution during alpha-beta heat treatment of Ti-6Al-4V. Metallurgical and Materials Transactions A 34, 2377–2386.
Semiatin, S.L., Stefansson, N., Doherty, R.D., 2005. Prediction of the Kinetics of Static Globularization of Ti-6Al-4V. Metallurgical and Materials Transactions 36A, 1372–1376.
Seshacharyulu, T., Medeiros, S.C., Frazier, W.G., Prasad, Y.V.R.K., 2002. Microstructural mechanisms during hot working of commercial grade Ti-6Al-4V with lamellar starting structure, vol. 325, pp. 112.
Shafaat, M.A., Omidvar, H., Fallah, B., 2011. Prediction of hot compression flow curves of Ti-6Al-4V alloy in $\alpha + \beta$ phase region. Materials & Design 32, 4689–4695.
Shewmon, P.G., 1963. Diffusion in solids. McGraw-Hill Series in Materials Science and Engineering. McGraw-Hill.
Simo, J., Hughes, T.J.R., 1998. Computational Inelasticity, . Interdisciplinary Applied Mathematics, first ed., 7. Springer.
Simo, J.C., Taylor, R.L., 1986. A return mapping algorithm for plane stress elastoplasticity. International Journal for Numerical Methods in Engineering 22, 649–670.
Stefansson, N., Semiatin, S.L., 2003. Mechanisms of globularization of Ti-6Al-4V during static heat treatment. Metallurgical and Materials Transactions 34A, 691–698.
Tersing, H., Lorentzon, J., Francois, A., Lundbäck, A., Babu, B., Barboza, J., Bäcker, V., Lindgren, L.E., 2012. Simulation of manufacturing chain of a titanium aerospace component with experimental validation. Finite Elements in Analysis and Design 51, 10–21.
Thomas, J.P., Semiatin, S.L., 2006. Mesoscale Modeling of the Recrystallization of Waspaloy and Application to the Simulation of the Ingot-Cogging Process. Technical Report AFRL-ML-WP-TP-2006-483. Materials and Manufacturing Directorate. Air Force Research Laboratory, Air Force Materiel Command, Wright-Patterson AFB, OH 45433–7750.

Tiley, J.S., 2002. Modeling of Microstructure Property Relationships in Ti-6Al-4V. Ph.D. thesis, Ohio State University.
Yeom, J.T., Kim, J.H., Kim, N.Y., Park, N.K., Lee, C.S., 2007. Characterization of dynamic globularization behavior during hot working of Ti-6Al-4V alloy. Advanced Materials Research 26–28, 1033–1036.
Zhao, W.J., Ding, H., Song, D., Cao, F., Hou, H.L., 2007. The Effect of Grain Size on Superplastic Deformation of Ti-6Al-4V Alloy. In: Zhang, K. (Ed.), Materials Science Forum, pp. 387–392.